Antiviral Research 102 (2014) 23–28

Contents lists available at ScienceDirect

Antiviral Research

journal homepage: www.elsevier.com/locate/antiviral

Naphthalene-sulfonate inhibitors of human norovirus RNA-dependent RNA-polymerase

Delia Tarantino [a], Margherita Pezzullo [a,b], Eloise Mastrangelo [a,b], Romina Croci [a], Jacques Rohayem [c,d], Ivonne Robel [d], Martino Bolognesi [a], Mario Milani [a,b,*]

[a] Department of Biosciences and CIMAINA, University of Milano, Via Celoria 26, I-20133 Milano, Italy
[b] CNR-IBF, Istituto di Biofisica, Via Celoria 26, I-20133 Milano, Italy
[c] Institute of Virology, Dresden University of Technology, Fiedlerstrasse 42, 01307 Dresden, Germany
[d] Riboxx GmbH, Pharmapark Radebeul, Meissner Strasse 191, 01445 Radebeul, Germany

ARTICLE INFO

Article history:
Received 24 July 2013
Revised 31 October 2013
Accepted 28 November 2013
Available online 4 December 2013

Keywords:
Norovirus
Caliciviridae
RNA-dependent RNA polymerase
Antiviral discovery
X-ray crystallography
Naphthalene-sulfonate

ABSTRACT

Noroviruses are members of the *Caliciviridae* family of positive sense RNA viruses. In humans Noroviruses cause rapid onset diarrhea and vomiting. Currently Norovirus infection is responsible for 21 million gastroenteritis yearly cases in the USA. Nevertheless, despite the obvious public health and socio-economic relevance, no effective vaccines/antivirals are yet available to treat Norovirus infection.

Since the activity of RNA-dependent RNA polymerase (RdRp) plays a key role in genome replication and in the synthesis/amplification of subgenomic RNA, the enzyme is considered a promising target for antiviral drug development. In this context, following the identification of suramin and NF023 as Norovirus RdRp inhibitors, we analyzed the potential inhibitory role of naphthalene di-sulfonate (NAF2), a fragment derived from these two molecules. Although NAF2, tested in enzymatic polymerase inhibition assays, displayed low activity against RdRp (IC_{50} = 14 μM), the crystal structure of human Norovirus RdRp revealed a thumb domain NAF2 binding site that differs from that characterized for NF023/suramin. To further map the new potential inhibitory site, we focused on the structurally related molecule pyridoxal-5′-phosphate-6-(2′-naphthylazo-6′-nitro-4′,8′-disulfonate) tetrasodium salt (PPNDS). PPNDS displayed below-micromolar inhibitory activity *versus* human Norovirus RdRp (IC_{50} = 0.45 μM), similarly to suramin and NF023. Inspection of the crystal structure of the RdRp/PPNDS complex showed that the inhibitor bound to the NAF2 thumb domain site, highlighting the relevance of such new binding site for exploiting Norovirus RdRp inhibitors.

© 2013 Elsevier B.V. All rights reserved.

1. Introduction

Noroviruses (NVs) are members of the *Caliciviridae* family of positive sense RNA viruses (Fauquet and Fargette, 2005; Green, 2007; Green et al., 2000; Mayo, 2002). Norovirus-linked gastroenteritis is estimated to affect ~21 million people annually in the United States, being responsible for up to 200,000 deaths per year in developing countries (Patel et al., 2008). The disease is usually acute and self-limiting, but in immunocompromised adults it can become chronic and persist for weeks–years (Bok and Green, 2012).

The NV genome (7.7 kb) contains three open reading frames (ORF1-3) of single stranded RNA. ORF1 is translated into a large polyprotein precursor, cleaved into six non-structural proteins (NS1–2, NS3, NS4, NS5, NS6 and NS7) by the viral protease (NS6); ORF2 and ORF3 encode for the capsid proteins VP1 and VP2, respectively (Clarke and Lambden, 2000). The structural and non-structural viral proteins that orchestrate the viral replicative machinery are potentially vulnerable targets for "attack" by proper ligands interfering with their functionality (Rohayem et al., 2010). The virus-specific nature of such targets, and their indispensable functions, provide the potential for limiting negative side effects of antiviral drugs on the physiologic host-cell processes.

In this context, we formerly identified suramin and the analogous compound NF023 as human and murine NV NS7 RNA-dependent RNA-polymerase (hNV- and mNV-RdRp, respectively) inhibitors (Mastrangelo et al., 2012). Our crystallographic analyses

Abbreviations: hNV, human Norovirus; mNV, murine Norovirus; RdRp, RNA-dependent RNA-polymerase; PDB, protein data bank; NAF2, naphthalene-1,5-disulfonic acid; PPNDS, pyridoxal-5′-phosphate-6-(2′-naphthylazo-6′-nitro-4′,8′-disulfonate) tetrasodium salt.

* Corresponding author at: CNR-IBF, Department of Biosciences, University of Milano Via Celoria 26, 20133 Milano, Italy. Tel.: +39 02 50314898; fax: +39 02 50314895.
E-mail address: mario.milani@unimi.it (M. Milani).

0166-3542/$ - see front matter © 2013 Elsevier B.V. All rights reserved.
http://dx.doi.org/10.1016/j.antiviral.2013.11.016

showed that the two inhibitors bind in an extended conformation to a common site, close to the enzyme catalytic center. Suramin and derivatives display poor membrane permeability (Beindl et al., 1996; Charlton et al., 1996; Klinger et al., 2001) due to the negative charges of their sulfonate groups, and would require chemical optimization to improve their drug-likeness. On the other hand, the suramin/NF023 binding site is located along the access pathway of incoming nucleoside triphosphates (NTPs) and is lined, in its central region, with lysine and arginine residues endowed with highly mobile side chains. Such conformational flexibility of the targeted binding site adds substantial complexity to the structure-based inhibitor optimization process. On such bases, we set out to investigate a fragment of the two mentioned inhibitors that, according to our crystal structures, mapped to the less flexible region (i.e. inner in the enzyme active site) of the suramin/NF023 binding site, likely representing their most inhibitory-active portion. We thus focused on naphthalene-1,5-disulphonic acid (NAF2; Fig. 1a) as a fragment of both suramin and NF023 'inhibitory heads', applying a sort of reverse fragment screening approach.

NAF2 was initially tested in enzymatic assays for inhibition of hNV-RdRp, showing modest activity (IC_{50} = 14 μM). Unexpectedly, however, the crystal structure of the hNV-RdRp/NAF2 complex showed that, besides the site previously characterized in the suramin/NF023 complexes, the compound bound also to a new thumb domain site, located in a cleft along the newly synthesized RNA exit path. Accordingly, the two NAF2 binding sites identified were named A-site ('old' site, common with suramin/NF023) and B-site ('new' site). In order to further characterize the B-site in view of its exploitation for inhibitor design, we then selected the NAF2 analog pyridoxal-5′-phosphate-6-(2′-naphthylazo-6′-nitro-4′,8′-disulfonate) tetrasodium salt (PPNDS, Fig. 1b), which our previous docking searches showed to potentially map to a region close to the B-site (Mastrangelo et al., 2012). PPNDS proved able to inhibit hNV-RdRp activity with an IC_{50} value in the sub-micromolar range (IC_{50} = 0.45 μM). Moreover, the crystal structure of the hNV-RdRp/PPNDS complex showed that the inhibitor indeed bound to the B-site previously mapped by NAF2. Our findings highlight a new RdRp inhibitory sub-site, and suggest that structure-based optimization of PPNDS may provide analogs with enhanced drug-likeness, shedding new light on the path towards anti-Norovirus drugs.

2. Materials and methods

2.1. Chemicals

For the RdRp inhibition assays poly(C) and the NAF2 compound were purchased from Sigma–Aldrich, while PPNDS was from Santa Cruz Biotechnology. The compounds were dissolved at 100 mM in H_2O and stored at −20 °C.

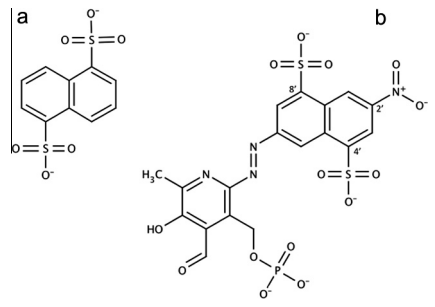

Fig. 1. Chemical structure of NAF2 (a) and PPNDS (b).

2.2. Expression and purification of the hNV-RdRp

hNV-RdRp was expressed in *Escherichia coli* and purified as previously described (Fullerton et al., 2007). The protein was dialyzed against buffer A (25 mM Tris/HCl, pH 7.4, 1 mM DTT, 100 mM NaCl, 1 mM EDTA) and concentrated to 9 mg/ml. Protein concentration was determined with the BCA Protein assay kit (Pierce) based on the Biuret reaction.

2.3. hNV-RdRp inhibition assays

In vitro RNA synthesis assays were performed as described (Mastrangelo et al., 2012). In brief the reaction mixture contained 20 mM Tris/HCl (pH 7.5), 1 mM DTT, 25 mM NaCl, 5 mM $MgCl_2$, 0.3 mM $MnCl_2$, 2 U RiboLock Ribonuclease inhibitor, PicoGreen Quantitation Reagent, and as substrates poly(C) template annealed with oligo$(G)_{12}$ primer (62.5 nM final concentration), and 100 μM GTP. Before starting the reaction, 1 μl of the protein was incubated for 5 min in the presence of 1 μl of water or 1 μl of one inhibitor solution at the required concentration. The reaction was started by the addition of the reaction mixture to the incubated protein (final protein concentration 255 nM; inhibitor concentration from 0 to 20 μM for NAF2, and from 0 to 10 μM for PPNDS) up to a total volume of 200 μl. The reactions were followed for 10 min at 30 °C recording (every 30 s) the fluorescence signals of the samples (in a Varian Cary Eclipse Fluorescence Spectrophotometer) arising from the interaction of the PicoGreen dye with the growing dsRNA. Protein activity was evaluated subtracting the slope of the linearly growing fluorescence from that of the same reaction mix win the absence of the enzyme. The results of three independent experiments were averaged. A plot of activity *versus* inhibitor concentration was used to estimate the IC_{50} values for each inhibitor (Table 1; Fig. S1) using the program GraFit (Erithacus software) or QtiPlot, using the four parameter equation:

$$A = m + (M - m)\frac{1}{1 + \left(\frac{[I]}{IC_{50}}\right)^{n}}$$

where A = activity, M = maximum activity, m = minimum activity, $[I]$=inhibitor concentration, n = Hill coefficient (Prinz, 2010).

Independently, kinetic experiments were performed in order to determine the PPNDS hNV RdRp inhibition mechanism relative to the poly(C)/oligo$(G)_{12}$ substrate. Briefly, to explore the inhibition mode, we performed standard enzymatic reactions for which the poly(C)/oligo$(G)_{12}$ concentration was varied (from 3.9 to 125 nM), at 100 μM GTP constant concentration, applying increasing amounts of the inhibitor (from 0 to 1 μM). The assays were performed using a TECAN Infinite 200 PRO microplate reader; the results were analyzed through Lineweaver–Burk plots ($1/V$ *versus* $1/[S]$) at varying PPNDS concentrations.

2.4. Biophysical characterization of the hNV-RdRp/inhibitor interaction

Thermofluorimetric (Thermal shift) assays for the evaluation of the hNV-RdRp melting temperature (T_m) in the absence/presence of the inhibitors were conducted in a MiniOpticon Real Time PCR Detection System (Bio-Rad), using the fluorescent dye Sypro Orange. 4 μl aliquots of hNV-RdRp solution (final protein concentra-

Table 1
IC_{50} values of the different compounds against hNV-RdRp.

Cpd	hNV-RdRp IC_{50} (μM)
Suramin	0.24 ± 0.08
NAF2	14.0 ± 1.0
PPNDS	0.45 ± 0.09

tion 34.7 μM) were diluted in 18 μl of its buffer, and mixed with 3.5 μl of Sypro orange (Sigma) diluted 60×, and PPNDS (5 or 50 μM), or 700 μM NAF2. In control samples the inhibitor solutions were replaced by water. The sample plates were heated from 20 to 90 °C, with a heating rate of 0.2 °C/min. Fluorescence intensities were measured within excitation/emission ranges of 470–505 nm and 540–700 nm, respectively.

2.5. Crystallization of the hNV-RdRp in presence of NAF2 and PPNDS

Sitting drop crystallization experiments for hNV-RdRp (11 mg/ml stock enzyme concentration) were assembled using an Oryx-8 crystallization robot (Douglas Instruments, East Garston, UK), from a 50%, 67%, 80% mixture of the protein with the reservoir solution (final drop volume 0.3 μl). Crystals grew in about 4 weeks, at 20 °C, in 1.2 M Na citrate, 100 mM Na cacodylate, pH 6.2, NaCl 125 mM. Before X-ray data collection, crystals were soaked in a cryoprotectant solution (1.4 M Na citrate, 100 mM Na cacodylate pH 6.2, and 25% glycerol) containing 30 mM NAF2, for 24 h, or containing 5 mM of PPNDS, 62.5 nM dsRNA (poly(C)/oligo$(G)_{12}$) and 100 μM GTP, for 36 h. The soaked crystals were then flash-cooled in liquid nitrogen. The hNV-RdRp/NAF2 crystals diffracted to a maximum resolution of 2.04 Å at the Elettra Synchrotron source (Trieste, Italy), beam line XRD1. The hNV-RdRp/PPNDS crystals diffracted to a maximum resolution of 2.6 Å at the ESRF Synchrotron facility (Grenoble, France), beam line ID29.

hNV-RdRp/NAF2 X-ray diffraction data were indexed using MOSFLM (Read et al., 2007), and intensities were merged using SCALA (Evans, 2006). hNV-RdRp/PPNDS X-ray diffraction data were indexed and scaled using XDS (Kabsch, 2010). The hNV-RdRp crystals grown in the presence both of NAF2 or PPNDS display closely similar unit cells and belong to the orthorhombic space group *I222*; data collection statistics are reported in Table 2.

Table 2
X-ray data-collection and refinement statistics for hNV-RdRp/NAF2 and for hNV-RdRp/PPNDS.

Protein	hNV-RdRp/NAF2	hNV-RdRp/PPNDS
Soaked compound	NAF2, 30 mM	PPNDS, 5 mM
Ligand site(s) present	A-site, B-site	B-site
Beam line & wavelength (Å)	ELETTRA XRD1 1.000	ESRF ID29 1.072
Space group	I222	I222
Unit-cell parameters (Å)	a = 86.6; b = 111.8; c = 121.4	a = 85.8; b = 116.1; c = 122.1
Molecules in a.u.	1	1
Resolution (Å)	45.4–2.04	38.4–2.6
Mosaicity (°)	0.6	0.4
Measured reflections	138,897 (20,166)[a]	87,361 (6,478)[c]
Unique reflections	37,405 (5,330)	19,046 (1,383)
Completeness (%)	98.7 (97.7)	99.6 (99.7)
Redundancy	3.7 (3.8)	4.6 (4.7)
R_{merge}[a] (%)	10.3 (41.7)	10.4 (73.8)
Average I/σ (I)	9.1 (2.7)	12.1 (1.9)
R_{factor}[b]/R free[c] (%)	17.0/22.3	22.0/28.5
r.m.s. Bonds (Å)	0.010	0.008
r.m.s. Angles (°)	1.37	1.18
Average protein B fac. (Å^2)	22.4	57.5
Average ligand B fac. (Å^2)	B-site = 20.9 A-site = 32.2	B-site = 85.2
Residues in most favored regions (%)	93.4	91.8
Residues in additionally allowed regions (%)	6.6	8.2
PDB-ID	4LQ9	4LQ3

Values in parentheses are for the highest resolution shell: [a](2.15–2.04); [b](2.66–2.60).

[a] $R_{merge} = \Sigma|I-(I)|/\Sigma I \times 100$, where I is intensity of a reflection and (I) is its average intensity.

[b] $R_{factor} = \Sigma||F_o|-|F_c||/\Sigma|F_o| \times 100$.

[c] R_{free} is calculated on 5% randomly selected reflections, for cross-validation.

2.6. Structure determination and refinement

The three-dimensional structures of hNV-RdRp in the complexes with NAF2 and PPNDS were solved by the Molecular Replacement method using the program MOLREP (Vagin and Teplyakov, 1997) and a search model based on the structure of the hNV-RdRp from strain Hu/NLV/Dresden174/1997/GE (PDB-id 2B43). The single molecule present in the crystal asymmetric unit was subjected to rigid-body refinement, and subsequently to constrained refined using REFMAC5 (Steiner et al., 2003). A random set comprising 5% of the data was omitted from refinement for R-free calculation. Manual rebuilding with COOT (Emsley et al., 2010); additional refinement with BUSTER (Smart et al., 2012) and REFMAC5, were subsequently performed, as needed. Refinement statistics as well as stereochemical quality assessment of the 3D structures are summarized in Table 2. Atomic coordinates and structure factors for hNV-RdRp in complex with NAF2 and PPNDS have been deposited with the PDB (Berman et al., 2000) with accession codes 4LQ9 and 4LQ3, respectively.

3. Results

3.1. In vitro inhibition of hNV-RdRp

In vitro RNA synthesis assays were performed using annealed poly(C)–oligo$(G)_{12}$ (62.5 nM final concentration) and GTP (100 μM final concentration), as polymerase substrates, and 255 nM RdRp, following procedures previously described (Mastrangelo et al., 2012). Under these experimental conditions, NAF2 inhibited hNV-RdRp activity with IC_{50} = 14 μM whereas PPNDS inhibited the enzyme with an IC_{50} value of about 0.45 μM (Table 1; Fig. S1). Furthermore, analyzing the dose–response curves for NAF2, it is evident that the number of bound inhibitor molecules is higher than 1 (Prinz, 2010). As described in the next paragraph, such value is in agreement with the crystal structure data, where we observed two ligand binding sites (see below).

We also analyzed the kinetic mechanism of hNV-RdRp inhibition by PPNDS (Fig. 2). The Lineweaver–Burk plots highlighted a non-competitive inhibition mechanism with respect to the poly(C)/oligo$(G)_{12}$ substrate, with a *Ki* value of 0.52 ± 0.05 μM, indicating that the inhibitor is able to bind to the free enzyme as well as to the enzyme–substrate complex.

In order to verify whether the selected compounds might induce some form of destabilization/denaturation of the enzyme, generally reflected by a variation of the protein T_m, we performed thermofluorimetric assays. The acquired data showed that hNV-RdRp displays the same T_m in the absence (T_m = 36.9 ± 0.5 °C) or in the presence of NAF2 (0.7 mM; T_m = 37.5 ± 0.4 °C). The thermofluorimetric signal recorded in the presence of PPNDS is markedly reduced when the inhibitor concentration is raised, since the red colored inhibitor molecule absorbs part of the incident radiation (in the 470–505 nm range). We were however able to test the effects on T_m at two PPNDS concentrations (5 and 50 μM), resulting in T_m values of 37.0 ± 0.5 and 41.0 ± 2.0, respectively (Fig. S2a and b). Despite the low fluorescence signal recorded in the presence of 50 μM PPNDS, the slight Tm increase observed would imply some protein stabilization induced by the bound inhibitor. All the thermofluorimetric results prove that the hNV-RdRp inhibition is not due to inhibitor-linked adverse effects on enzyme stability/denaturation.

3.2. Crystal structures of hNV-RdRp with NAF2

3.2.1. Inhibitor binding to the B-site

The analysis of NAF2 binding to the RdRp domain was addressed through X-ray crystallography. To this purpose,

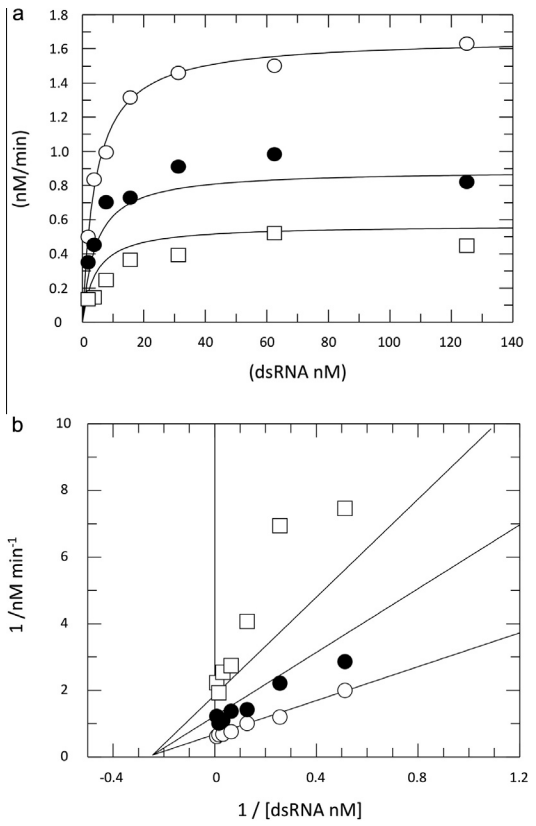

Fig. 2. (a) Reaction velocity plot as a function of the RNA concentration, ○ in absence of the inhibitor, ● in presence of 0.45 μM of PPNDS and □ in presence of 1 μM of PPNDS. (b) Lineweaver–Burk double reciprocal plot for the non competitive inhibition mechanism of hNV RdRp activity by PPNDS, relative to RNA substrate.

hNV-RdRp crystallization experiments were performed in presence of NAF2 (see Section 2for details). The hNV-RdRp crystals were soaked in 30 mM NAF2 before cryo-cooling, The crystal (belonging to the orthorhombic space group *I222*, with one molecule per asymmetric unit) diffracted to a maximum resolution of 2.04 Å, and the structure was refined to a final crystallographic R-factor of 17.0% and R-free of 22.3% (Table 2). The first refinement cycles showed residual electron density compatible with a NAF2 molecule located in a positively charged cleft within the thumb domain (Fig. 3a and b), built by an α-β-loop-α motif; inspection of the enzyme structure confirms that this site (hereafter, the B-site) is different from the binding site where suramin and NF023 inhibitors were located (hereafter, the A-site). In the B-site, the negative charges of NAF2 sulfonates are balanced by Arg419 and Arg436; the naphthalene ring is sandwiched between Gln414 and Gln439 (forming an intertwined hydrogen bond network together with Asn505), on one side, and Phe28 and Arg419, on the other (Fig. 3b). Additional polar interactions involve the side chains of Asn505 and Thr418 and the main chain nitrogen of Arg419. Inspection of the hNV-RdRp/NAF2 crystal structure in comparison to the enzyme 3D structure in the absence of inhibitors (pdb-id: 2B43, r.m.s.d. 0.70 Å, over 499 Cα pairs) shows that, upon NAF2 binding, the protein undergoes only slight structural rearrangements at a few residues, and at the last two C-terminal residues, Asn505 and Glu506, visible in the electron density.

3.2.2. Inhibitor binding to the A-site

Further inspection of difference Fourier maps revealed residual electron density compatible with one NAF2 molecule in the A-site (Fig. 3a and c), i.e. at a location very close to the site occupied by the naphthalene-sulfonate moiety of NF023/suramin, in the fingers domain (Fig. 3c; Mastrangelo et al., 2012). Lys171, Lys174, Lys180 and Arg182 stabilize the inhibitor negative charges; the sulfonate groups establish H-bonds with Gln66 and the main chain N atom of Lys171. Additionally, the naphthalene ring makes π-cation interactions with Lys174 and Arg182 (Fig. 3c).

3.3. Crystal structure of hNV-RdRp bound to PPNDS

In a previous virtual screening search targeting a wide region around the hNV-RdRp active site, we identified PPNDS, a compound hosting a naphthalene disulfonate moiety, among other potential NV-RdRp inhibitors (Mastrangelo et al. 2012). Analysis of the simulated structure showed that PPNDS would locate in a

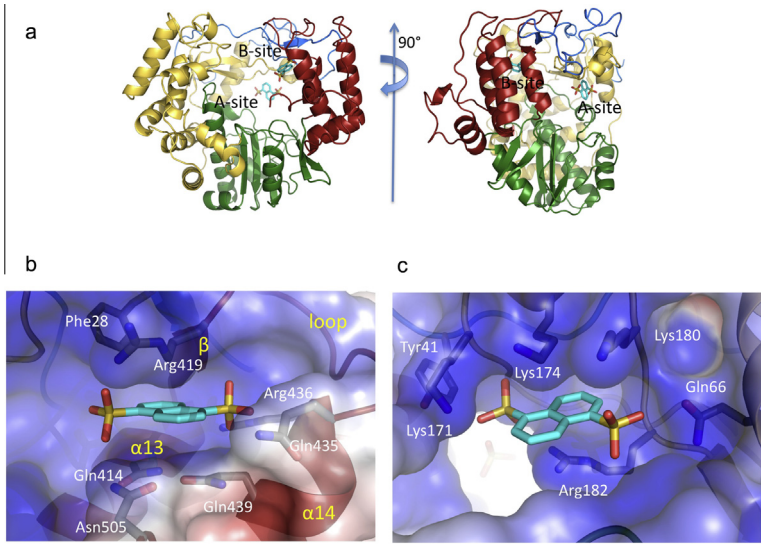

Fig. 3. (a) Crystal structure of hNV-RdRp bound to two NAF2 molecules in the A-site and B-site; the overall structure of hNV-RdRp in cartoon: N-terminal domain (blue), thumb (red), fingers (yellow) and palm (green). The picture on the right is rotated by 90 degree around the vertical axis. (b and c) Details of the hNV-RdRp/NAF2 interaction in the B-site (b) and A-site (c); transparent surface colored by electrostatic potential (program APBS2; (Baker et al., 2001)); amino acids involved in the interaction with NAF2 are labeled. Figures created using PyMol (http://www.pymol.org). (For interpretation of the references to color in this figure legend, the reader is referred to the web version of this article.)

region close to the B-site described above. Therefore, for the present study, PPNDS was selected as a commercially available compound potentially useful to further characterize structural features of the newly identified B-site. Notably, we succeeded in obtaining crystals of hNV-RdRp bound to PPNDS only after soaking the protein with the inhibitor in the presence of dsRNA and GTP (see Section 2.5 for details). This suggests that inhibitor binding to the protein requires local structural changes related to events in the catalytic cycle. The protein crystal structure was refined to a final crystallographic *R*-factor of 22.0%, and *R*-free of 28.5%, for the 2.6 Å resolution data set (Table 2). As predicted by the docking study, PPNDS binds only to the B-site (Fig. 4, Fig. S3a and b). The overall structure of the whole enzyme bound to PPNDS appears slightly more compact relative to that of the inhibitor-free protein (pdb-id 1SH0; r.m.s.d. 1.01 Å, over 484 Cα pairs (Ng et al., 2004)). Such overall effect is related to a small displacement of both the fingers and the thumb domains toward the active site, as in a closing hand, and is likely due to the interaction of the protein with dsRNA (Fig. 4a and b). In fact, the crystal structure shows residual electron density hosted between the fingers and thumb domains compatible with two or three RNA nucleotides, which have been only partially modeled in the refined structure, due to electron density ambiguities. The nucleotides are hosted in a positively charged region along the exit pathway of the newly formed RNA chain (Zamyatkin et al., 2008).

The PPNDS molecule can be schematically divided into two moieties, the naphthalene 6′-nitro-4′,8′-disulfonate and the pyridoxal-5′-phosphate, linked by the azo bond (Fig. 1b). The nitro group of the first moiety is tightly hosted in a hydrophobic cleft, between helices α13 and α14 of the thumb domain, lined with Leu406, Ile411 (α13), Leu443 (α14), Val504 (C-terminal) and with the aliphatic portion of the side chains of Ser 410 (α13), Gln414 (α13) and Glu446 (α14) (Fig. 4c, Fig. S3b). Both PPNDS sulfonate groups point toward the solvent; the 8′ sulfonate establishes hydrogen bonds with Gln414 and Gln439, while the 4’ sulfonate is H-bonded to Ser410 and salt bridges with Arg413 and Arg392 (Fig. 4c). The naphthalene ring is in van der Waals contacts with Gln414. The PPNDS pyridoxal-5′-phosphate group is elongated toward the fingers domain, stabilizing the conformation of the C-ter end of hNV-RdRp within the active site cavity (Fig. 4a and c). In fact, while in the inhibitor-free enzyme the C-ter is modeled in the electron density up to Glu506–Asp507, when PPNDS is present all the C-ter residues can be modeled (Glu510 is in van der Waals contact with the pyridoxal moiety, and H-bonded to its phosphate group). Interestingly, the PPNDS phosphate group points toward the active site region in the palm domain, which is rich in negatively charged amino acids, partially masked by Arg182, Arg392 and Mg^{2+}. Finally, the carbonyl group of the pyridoxal ring is H-bonded to Glu168. Relative to NAF2, the PPNDS molecule appears to be shifted toward the palm domain of about two α helical turns (~6–7 Å) along the direction of the antiparallel helices α13 and α14. Such PPNDS location may be dictated by the nitro group that cannot be properly hosted in the NAF2 cavity due to clash with Trp417 main chain (in the α13-β motif of the thumb domain). Notably, the location of PPNDS at a site different from the previously identified A-site is independently assessed by the close matching of the IC_{50} values obtained (as described above) for w.t. hNV-RdRp (Table 1) and for its Y41A mutant, where a key residue building the A-site is replaced by Ala (IC_{50} of about 500 ± 50 nM). In fact, such a mutation was previously shown to affect suramin and NF023 inhibitory effects on hNV-RdRp (Mastrangelo et al., 2012).

4. Discussion

In a previous work (Mastrangelo et al., 2012) we showed that suramin and NF023 binding site to mNV-RdRp, and to hNV-RdRp, as inferred by crystal structures and mutation analysis, is located along the access pathway of NTPs to the enzyme active center. Accordingly, such site is lined with positively charged residues whose conformational flexibility helps promoting the diffusion of NTPs toward the catalytic site. Such structural features are unlikely to make this inhibitor binding site an ideal target region for structure based drug optimization. We therefore decided to analyze the structural and inhibitory properties of fragments of the

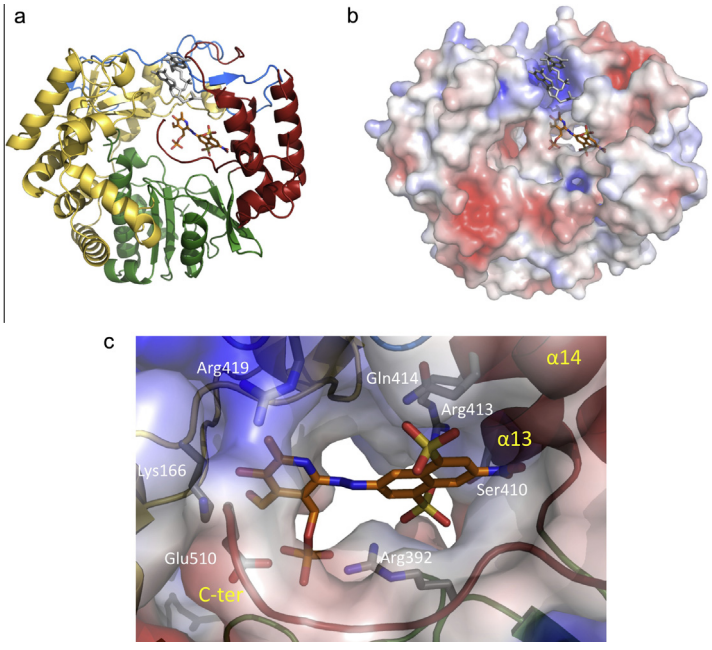

Fig. 4. (a) Crystal structure of hNV-RdRp bound to PPNDS in cartoon. PPNDS (orange carbon atoms) and a fragment of ssRNA, partially modeled into observed electron density (gray) are shown as sticks. (b) Same as (a) with protein surface colored by electrostatic potential. (c) Details of the local contacts between PPNDS and hNV-RdRp; amino acids involved in the interaction with PPNDS are labeled. (For interpretation of the references to color in this figure legend, the reader is referred to the web version of this article.)

identified inhibitors, focusing on their naphthalene-sulfonate moieties, thus selecting the NAF2 compound. Enzymatic assays showed that the selected fragment of the initial inhibitors still retains marginal inhibitory activity. More importantly, besides the site previously characterized in the suramin/NF023 complexes (here identified as the A-site), such reverse fragment screening experiments unraveled a novel, unexpected, binding site for NAF2, located in the RdRp thumb domain (B-site). Interestingly, the B-site is located in a position that is roughly structurally equivalent to the benzothiadiazine inhibitor binding site in the Hepatitis C Virus RdRp (Koch and Narjes, 2006; Pfefferkorn et al., 2005). NAF2 binding to two distinct sites is also suggested by analysis of the inhibition mechanism which shows a Hill coefficient higher than 1. In order to further characterize the B-site we selected PPNDS, a naphthalene sulfonate-based compound that is a potent and selective P2X1 receptor antagonist (Lambrecht et al., 2000). We demonstrated that PPNDS is able to inhibit the polymerase activity (Hill coefficient ~1, Fig. S1b) with a potency close to that observed for suramin or NF023. The crystal structure of the hNV-RdRp/PPNDS complex shows that the compound is anchored to the protein mostly through its naphthalene moiety. On the other hand, the improved inhibitory efficacy is likely dependent on PPNDS pyridoxal moiety that extends toward the enzyme active site. Such consideration is in keeping with the fact that: (i) NAF2 does not exert considerable inhibition, and (ii) PPNDS helps fixing the C-terminal end of the enzyme inside the active site, likely blocking the access of both the ssRNA template and the NTPs. The discovery of a new inhibitor binding site, and our analysis of the PPNDS binding mode to hNV-RdRp, provide new structural bases for modification of PPNDS and/or related compounds, in order to improve its efficacy and drug-likeness.

Acknowledgment

This work was funded by the FP7 HEALTH-2010 Collaborative Project SILVER (No. 260644).

Appendix A. Supplementary data

Supplementary data associated with this article can be found, in the online version, at http://dx.doi.org/10.1016/j.antiviral.2013.11.016.

References

Baker, N.A., Sept, D., Joseph, S., Holst, M.J., McCammon, J.A., 2001. Electrostatics of nanosystems: application to microtubules and the ribosome. Proc. Natl. Acad. Sci. USA 98, 10037–10041.

Beindl, W., Mitterauer, T., Hohenegger, M., Ijzerman, A.P., Nanoff, C., Freissmuth, M., 1996. Inhibition of receptor/G protein coupling by suramin analogues. Mol. Pharmacol. 50, 415–423.

Berman, H.M., Westbrook, J., Feng, Z., Gilliland, G., Bhat, T.N., Weissig, H., Shindyalov, I.N., Bourne, P.E., 2000. The protein data bank. Nucleic Acids Res. 28, 235–242.

Bok, K., Green, K.Y., 2012. Norovirus gastroenteritis in immunocompromised patients. N. Engl. J. Med. 367, 2126–2132.

Charlton, S.J., Brown, C.A., Weisman, G.A., Turner, J.T., Erb, L., Boarder, M.R., 1996. PPADS and suramin as antagonists at cloned P2Y- and P2U-purinoceptors. Br. J. Pharmacol. 118, 704–710.

Clarke, I.N., Lambden, P.R., 2000. Organization and expression of calicivirus genes. J. Infect. Dis. 181 (Suppl. 2), S309–316.

Emsley, P., Lohkamp, B., Scott, W.G., Cowtan, K., 2010. Features and development of Coot. Acta Crystallogr. Sect. D 66, 486–501.

Evans, P., 2006. Scaling and assessment of data quality. Acta Crystallogr. D: Biol. Crystallogr. 62, 72–82.

Fauquet, C.M., Fargette, D., 2005. International committee on taxonomy of viruses and the 3,142 unassigned species. Virol. J. 2, 64.

Fullerton, S.W., Blaschke, M., Coutard, B., Gebhardt, J., Gorbalenya, A., Canard, B., Tucker, P.A., Rohayem, J., 2007. Structural and functional characterization of sapovirus RNA-dependent RNA polymerase. J. Virol. 81, 1858–1871.

Green, K.Y., 2007. Caliciviridae: the noroviruses. In: Knipe, D.M., Howley, P.M. (Eds.), fifth 144 ed. Fields Virology, vol. 1. Lippincott Williams & Wilkins, a 145 Wolters Kluwer Business, Philadelphia, USA, pp. 41–51.

Green, K.Y., Ando, T., Balayan, M.S., Berke, T., Clarke, I.N., Estes, M.K., Matson, D.O., Nakata, S., Neill, J.D., Studdert, M.J., Thiel, H.J., 2000. Taxonomy of the *caliciviruses*. J. Infect. Dis. 181 (Suppl. 2), S322–330.

Kabsch, W., 2010. Xds. Acta Crystallogr. D: Biol. Crystallogr. 66, 125–132.

Klinger, M., Bofill-Cardona, E., Mayer, B., Nanoff, C., Freissmuth, M., Hohenegger, M., 2001. Suramin and the suramin analogue NF307 discriminate among calmodulin-binding sites. Biochem. J. 355, 827–833.

Koch, U., Narjes, F., 2006. Allosteric inhibition of the hepatitis C virus NS5B RNA dependent RNA polymerase. Infect. Disord. Drug Targets 6, 31–41.

Lambrecht, G., Rettinger, J., Baumert, H.G., Czeche, S., Damer, S., Ganso, M., Hildebrandt, C., Niebel, B., Spatz-Kumbel, G., Schmalzing, G., Mutschler, E., 2000. The novel pyridoxal-5′-phosphate derivative PPNDS potently antagonizes activation of P2X(1) receptors. Eur. J. Pharmacol. 387, R19–21.

Mastrangelo, E., Pezzullo, M., Tarantino, D., Petazzi, R., Germani, F., Kramer, D., Robel, I., Rohayem, J., Bolognesi, M., Milani, M., 2012. Structure-based inhibition of Norovirus RNA-dependent RNA polymerases. J. Mol. Biol. 419, 198–210.

Mayo, M.A., 2002. A summary of taxonomic changes recently approved by ICTV. Arch. Virol. 147, 1655–1663.

Ng, K.K., Pendas-Franco, N., Rojo, J., Boga, J.A., Machin, A., Alonso, J.M., Parra, F., 2004. Crystal structure of norwalk virus polymerase reveals the carboxyl terminus in the active site cleft. J. Biol. Chem. 279, 16638–16645.

Patel, M.M., Widdowson, M.A., Glass, R.I., Akazawa, K., Vinje, J., Parashar, U.D., 2008. Systematic literature review of role of noroviruses in sporadic gastroenteritis. Emerg. Infect. Dis. 14, 1224–1231.

Pfefferkorn, J.A., Greene, M.L., Nugent, R.A., Gross, R.J., Mitchell, M.A., Finzel, B.C., Harris, M.S., Wells, P.A., Shelly, J.A., Anstadt, R.A., Kilkuskie, R.E., Kopta, L.A., Schwende, F.J., 2005. Inhibitors of HCV NS5B polymerase. Part 1: Evaluation of the southern region of (2Z)-2-(benzoylamino)-3-(5-phenyl-2-furyl)acrylic acid. Bioorg. Med. Chem. Lett. 15, 2481–2486.

Prinz, H., 2010. Hill coefficients, dose–response curves and allosteric mechanisms. J. Chem. Biol. 3, 37–44.

Read, R., Sussman, J., Leslie, A.W., Powell, H., 2007. Processing Diffraction Data with Mosflm, Evolving Methods for Macromolecular Crystallography. Springer, Netherlands, pp. 41–51.

Rohayem, J., Bergmann, M., Gebhardt, J., Gould, E., Tucker, P., Mattevi, A., Unge, T., Hilgenfeld, R., Neyts, J., 2010. Antiviral strategies to control calicivirus infections. Antiviral Res. 87, 162–178.

Smart, O.S., Womack, T.O., Flensburg, C., Keller, P., Paciorek, W., Sharff, A., Vonrhein, C., Bricogne, G., 2012. Exploiting structure similarity in refinement: automated NCS and target-structure restraints in BUSTER. Acta Crystallogr. Sect. D 68, 368–380.

Steiner, R.A., Lebedev, A.A., Murshudov, G.N., 2003. Fisher's information in maximum-likelihood macromolecular crystallographic refinement. Acta Crystallogr. Sect. D 59, 2114–2124.

Vagin, A., Teplyakov, A., 1997. MOLREP: an automated program for molecular replacement. J. Appl. Crystallogr. 30, 1022–1025.

Zamyatkin, D.F., Parra, F., Alonso, J.M., Harki, D.A., Peterson, B.R., Grochulski, P., Ng, K.K., 2008. Structural insights into mechanisms of catalysis and inhibition in Norwalk virus polymerase. J. Biol. Chem. 283, 7705–7712.